Metamagnetism of few-layer topological antiferromagnets

C. Lei,[1] O. Heinonen,[2] A. H. MacDonald,[1] and R. J. McQueeney[3,4]
[1]*Department of Physics, The University of Texas at Austin, Austin, Texas 78712, USA*
[2]*Argonne National Laboratory, Lemont, Illinois 60439, USA*
[3]*Ames Laboratory, Ames, Iowa 50011, USA*
[4]*Department of Physics and Astronomy, Iowa State University, Ames, Iowa 50011, USA*

(Received 24 February 2021; accepted 25 May 2021; published 8 June 2021)

$MnBi_2Te_4$ (MBT) materials are a promising class of antiferromagnetic topological insulators whose films provide access to novel and technologically important topological phases, including quantum anomalous Hall states and axion insulators. MBT device behavior is expected to be sensitive to the various collinear and noncollinear magnetic phases that are accessible in applied magnetic fields. Here, we use classical Monte Carlo simulations and electronic structure models to calculate the ground state magnetic phase diagram as well as topological and optical properties for few-layer films with up to six septuple layers. Using magnetic interaction parameters appropriate for MBT, we find that it is possible to prepare a variety of different magnetic stacking sequences, some of which have sufficient symmetry to disallow nonreciprocal optical response and Hall transport coefficients. Other stacking arrangements do yield large Faraday and Kerr signals, even when the ground state Chern number vanishes.

DOI: 10.1103/PhysRevMaterials.5.064201

I. INTRODUCTION

$MnBi_2Te_4$ (MBT) is a promising platform for the development of unique devices based on topological electronic bands [1–28]. The utility of MBT is a consequence of its natural layered structure, which consists of stacks of ferromagnetic septuple layers (SLs) with out-of-plane magnetization and with inverted electronic bands with nontrivial topology [1–3]. There is great interest in controlling the sequence of magnetic and topological layers as a means to control phenomena related to the band topology [9]. Bulk MBT adopts a staggered antiferromagnetic (AF) stacking of the FM SLs [3,10,12,18] shown in Fig. 1, providing the first realization of an AF topological insulator, which is predicted to host unique axion electrodynamics [29,30]. Weak interlayer magnetic interactions across the van der Waals gap and uniaxial magnetic anisotropy allow for facile control of the magnetic structure. For example, a bulk Weyl semimetallic phase is predicted when all FM layers in MBT are field polarized with a small applied magnetic field [9,15,16].

Perhaps the most exciting opportunity in MBT materials is the possibility of developing thin film devices with precisely controlled magnetic stacking sequences. In this context, devices with even and odd numbers of AF stacked layers offer qualitatively different topological phase possibilities [11,23,28,31–33]. An odd number of magnetic layers necessarily has partially compensated magnetization that is beneficial for the observation of the quantum anomalous Hall (QAH) effect [11]. On the other hand, fully compensated magnetization occurs in even layer devices with zero applied magnetic field and provides an ideal platform to search for axion insulators with quantized magnetoelectric coupling [13,23]. However, there are also much richer possibilities in both odd or even layer samples [33] since the application of a magnetic field can result in different collinear magnetic stackings with partially compensated magnetization or even to noncollinear (canted) magnetic phases. The possibility to stabilize such phases and the potential for realizing unique topological phases in this scenario has not been considered.

The magnetization behavior of AF multilayers displays rich metamagnetic behavior with features, such as surface spin-flop transitions, that are not observed in bulk antiferromagnets [34,35]. This complex behavior is a consequence of competition between single-ion anisotropy, interlayer magnetic exchange, and Zeeman energy. For topological materials, whether the symmetry of different magnetic layer stacking sequences can affect the topological properties of the bands is an open question. For example, collinear metamagnetic phases with the same net magnetization can result from magnetic layer stackings that may or may not break inversion symmetry ($\mathcal{I}$). Here we use classical Monte Carlo simulations to show that it is generally possible to tune in different stacking sequences with distinct symmetries using an applied magnetic field. We find that realistic values of the single-ion anisotropy and exchange place MBT close to this tunability regime. Finally, we discuss the topological properties of accessible field-tuned states and strategies to identify them experimentally.

II. MONTE CARLO SIMULATIONS OF BULK $MnBi_2Te_4$

The spin lattice of MBT consists of triangular FM layers which are stacked in a close-packed fashion along the direction perpendicular to the layers. Interlayer interactions are

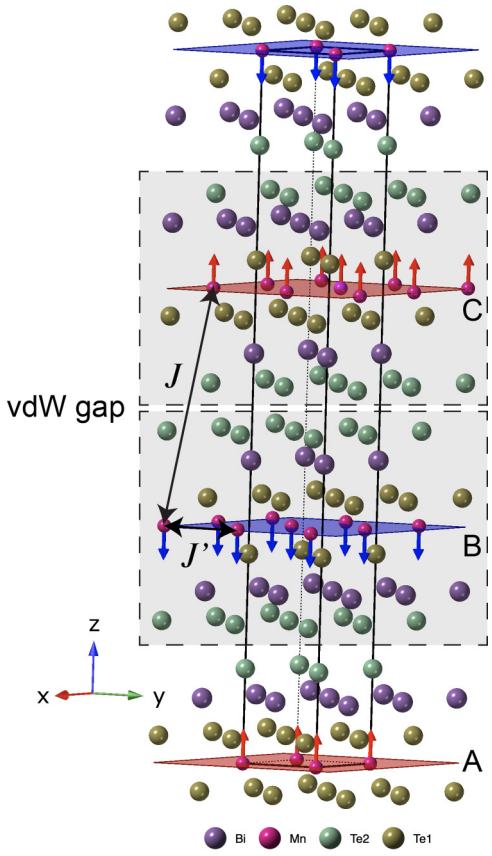

FIG. 1. Bulk crystal and magnetic structure of $MnBi_2Te_4$. Red and blue arrows and planes denote the ferromagnetic layers with staggered magnetization, forming an A-type structure. Gray rectangles identify septuple layers that are separated by a van der Waals (vdW) gap. Septuple layers are staggered in a close-packed ABC stacking. Principal antiferromagnetic interlayer (J) and ferromagnetic intralayer (J') interactions are indicated by black arrows.

antiferromagnetic, resulting in the zero-field A-type ground state [see the full and schematic structures in Figs. 1 and 2(a), respectively]. Magnetization and neutron diffraction experiments find Mn moments oriented perpendicular to the layers consistent with uniaxial magnetic anisotropy [18]. These features suggest that a simple spin model can be used to study the magnetization behavior of MBT in an applied magnetic field

$$H = J' \sum_{\langle ij \rangle ||} \mathbf{S}_i \cdot \mathbf{S}_j + J \sum_{\langle ij \rangle \perp} \mathbf{S}_i \cdot \mathbf{S}_j - D \sum_i S_{i,z}^2 - g\mu_B \mathbf{H} \cdot \sum_i \mathbf{S}_i. \quad (1)$$

Here, $\mathbf{S}_i$ is the Mn spin at site i ($S = 5/2$), $J' < 0$ is the intralayer FM exchange, $J > 0$ is the interlayer AF exchange, and D is the uniaxial single-ion anisotropy. Each Mn ion has six interlayer and intralayer nearest neighbors ($z = 6$). A representative and consistent set of coupling parameter values for MBT have been obtained from magnetization [18] and inelastic neutron scattering experiments [17]; $SJ' = -0.35$ meV, $SJ = 0.088$ meV, and $SD = 0.07$ meV.

Using these nominal values, classical Monte Carlo (MC) simulations on bulk and few-layer MBT systems have been performed using both UppASD [36] and Vampire [37] software packages. MC simulations are first performed on bulk MBT with a $21 \times 21 \times 12$ system size (14 553 spins) with periodic boundary conditions. MC simulations are run with the field pointed perpendicular to the layers using 50 000 MC steps per field to equilibrate the structure and an additional 20 000 steps to calculate the average magnetic properties. To account for hysteresis and history dependence, we begin the simulations with the field polarized state at $H = 12$ T and $T = 0.1$ K and ramp the field down in equal steps, using the final state from the previous field as the initial state for the current field.

Figure 2(b) summarizes typical MC simulation results for bulk MBT that reveal a Néel temperature of 22 K and magnetization curves with field-polarized saturation fields ($\mu_0 H_{ab}^{\text{sat}} = 10.3$ T and $\mu_0 H_c^{\text{sat}} = 7.9$ T), and a spin-flop field ($\mu_0 H_{\text{SF}} = 3.7$ T), in agreement with bulk measurements [10,12,18]. The hysteresis of the spin-flop transition is noticeably absent in the experimental data of bulk single crystals, which suggests that the spin-flop transition in real crystals does not occur by coherent layer rotation and could occur instead by surface nucleation [38].

For a general bulk uniaxial AF with a dominant FM intralayer coupling J', critical values of the ratio D/zJ determine the magnetization behavior when the field is applied along the c axis. Only three phases are possible: the AF phase, the canted spin-flop phase (SF), and the field-polarized phase (FM). For relatively weak anisotropy $D/zJ < 1/3$, a first-order spin-flop transition phase is expected, followed by a second-order transition to the field polarized state (AF $\rightarrow$ SF $\rightarrow$ FM). The nominal MBT parameters yield $D/zJ \approx 0.13$ which is well within the spin-flop regime. For dominant single-ion anisotropy $D/zJ > 1$, the virgin AF state is swept out by a weak applied field and a FM hysteresis loop develops. This behavior is observed in $MnBi_4Te_7$, in which the addition of a nonmagnetic Bi_2Te_3 spacer between $MnBi_2Te_4$ layers dramatically weakens the interlayer magnetic exchange [39,40]. In the intermediate regime $1/3 < D/zJ < 1$, the AF $\rightarrow$ FM transition occurs directly (a spin-*flip* transition), whereas the field-reversed transition goes through the spin-flop regime (FM $\rightarrow$ SF $\rightarrow$ AF).

III. FIELD-TUNED FEW-LAYER MAGNETIZATION

We now consider the behavior of the magnetization in thin film samples consisting of N magnetic layers, with $N = 3$, 4, 5, and 6. The phase diagram of N-layer systems is much more complex than the bulk phase diagram because regions of stability exist (as described in detail below) that correspond to collinear magnetic phases with partially compensated magnetization (ferrimagnetic phases). In this respect, significant differences occur between odd or even layer systems because the net magnetization cannot be fully compensated in odd layer films. Figures 2(c)–2(f) shows the magnetization for $N = 3$-, 4-, 5-, and 6-layer MBT obtained from MC simulations using a 11×11 system size for the basal layer and the nominal MBT Heisenberg parameters. Select simulations with a larger 21×21 basal layer produce no significant changes in the magnetization sweeps.

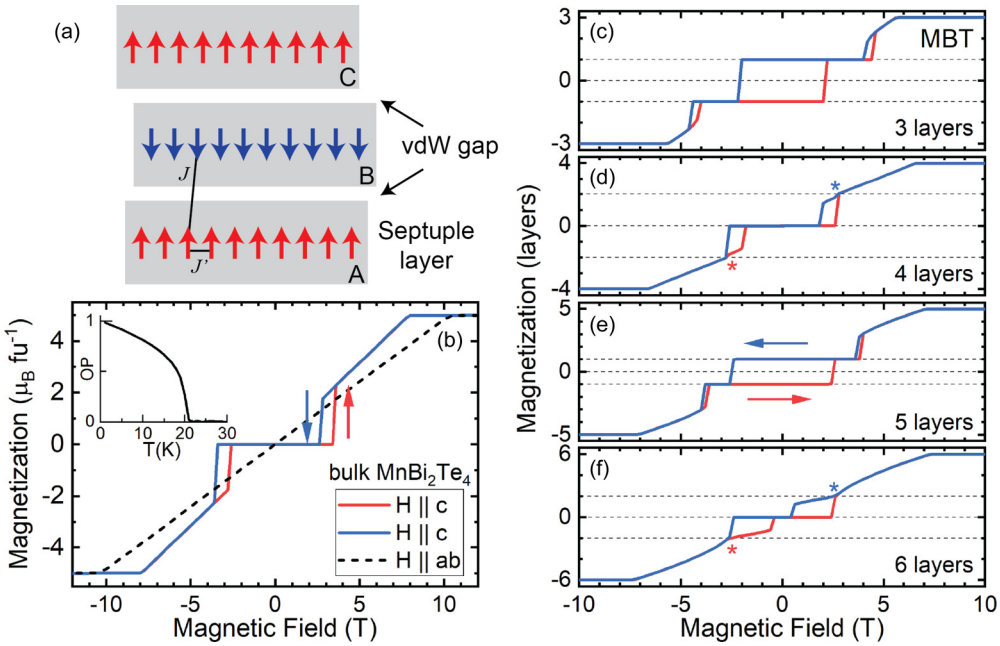

FIG. 2. (a) Schematic magnetic layer structure of MBT in the crystallographic unit cell with close-packed stacking of septuple blocks. The intralayer (J') and interlayer (J) magnetic interactions are indicated. The gray shaded boxes indicate the full septuple layers separated by a vdW gap. (b) Monte Carlo simulations of the bulk magnetization of MBT with field applied perpendicular and parallel to the Mn layers. Inset shows the order parameter (OP) of the staggered A-type AF order, which is defined as $(s_1 - s_2)/2$, with s_i the magnetization in each Mn layer, as a function of temperature. (c)–(f) Monte Carlo simulations of the magnetization of 3-, 4-, 5-, and 6-layer MBT, respectively, using the nominal Heisenberg parameters. For $N = 4$ and 6, the "$*$" indicates an additional phase transition.

For $N = 3$- and 5-layer simulations with the nominal MBT parameters, we find the expected FM hysteresis loop corresponding to the magnetization of a single uncompensated layer ($M = \pm 1$). In addition, we find a hysteretic spin-flop-like transition from the $M = \pm 1$ phase to the fully polarized FM phase. For $N = 4$ and $N = 6$, magnetization curves resemble bulk MBT with a AF $\rightarrow$ SF $\rightarrow$ FM sequence of transitions. However, one notices evidence for an additional transition [indicated with a "$*$" in Figs. 2(d) and 2(f)] within the spin-flop phase near 3 T. As we will show below, this transition demonstrates that the nominal parameters of MBT are close to a critical point in the phase diagram at which the $M = 2$ collinear phase becomes stable. We note that experimental evidence exists for $M = 2$ magnetization plateaus in the $N = 4$- and 6-layer films based on reflective magnetic circular dichroism experiments in some samples [32,33]. We hypothesize that sample-to-sample variations in the observed transport and magnetic properties of these films may be due to the combined role of defects, disorder, and the proximity of MBT to the $M = 2$ critical point. The experimental results in Refs. [32,33] are analyzed using numerical methods similar to the Mills model [41] described below.

To explore the nature of this critical point and parameter regimes beyond the nominal values chosen to represent MBT, we calculated the phase diagrams for the 3-, 4-, 5-, and 6-layer systems as a function of field and the single-ion anisotropy parameter (D), as shown in Fig. 3. Generally, these phase diagrams show regions of collinear magnetism separated by noncollinear (spin-flop-like) phases. For the largest uniaxial anisotropy values, the system approaches the behavior of a finite Ising chain where successive first-order transitions occur via random single-layer spin flips. We label the collinear ground state phases as AF ($M = 0$, $N = even$ only), Mn ($M = n$, with $n - 1$ broken AF bonds), and FM ($M = N$, field polarized with all AF bonds broken). Their time-reversed states are indicated by a bar (eg., $\overline{\text{M2}}$) and states that have identical ground state energies within our model, when they occur, are differentiated by a prime symbol (eg., M2′, M2″). Metastable excited states, when they occur, are labeled with an asterisk (e.g., M0*).

IV. METAMAGNETIC STATES

The distinct collinear ground states that occur for $N = 3$ and $N = 4$ are illustrated in Figs. 4(a) and 4(b). For $N = 4$, the MC phase diagram in Fig. 3(b) is consistent with the phase boundaries, critical points, and metastability limits obtained using the Mills model [35,41]. As expected, slightly increasing D from the nominal MBT value of $SD = 0.07$ meV stabilizes the M2 collinear phase, replacing the inflection in Fig. 2(d) with a magnetization plateau. Analysis of 4-layer Mills model reveals that this critical point occurs at $(SD, \mu_0 H)_\beta = (0.082 \text{ meV}, 3.59 \text{ T})$ [35].

For odd thin film thicknesses ($N = 3$ and 5), the magnetization sequence at low D/zJ reveals M1 and $\overline{\text{M1}}$ phases that form a hysteresis loop. For $N = 5$, larger D/zJ reveals two M3 states occur, labeled as M3′ and M3″ in Fig. 4(c), which have identical energies in our model but are distinguished by the presence (M3′) or absence (M3″) of mirror symmetry. Analysis of the sublattice magnetization from our simulations shows that only the mirror symmetric M3′ phase appears in the range of D/zJ studied.

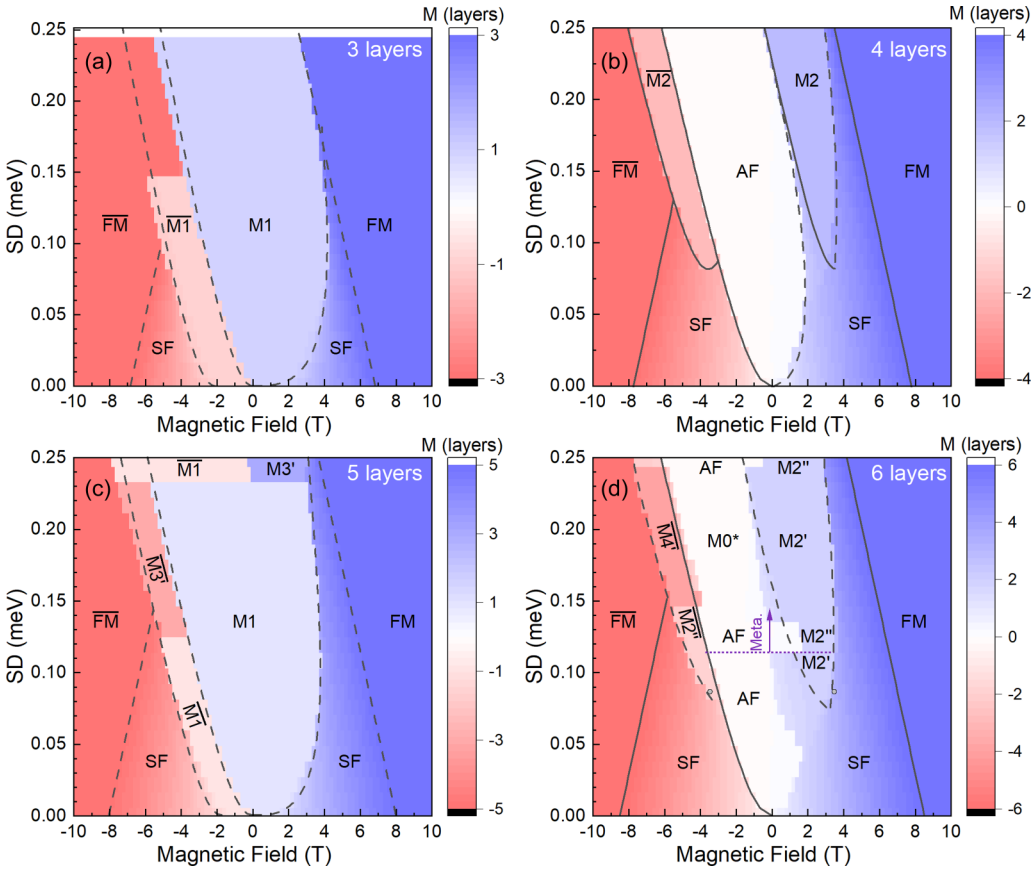

FIG. 3. Phase diagrams obtained by MC simulation showing the layer magnetization of a uniaxial layered antiferromagnet vs magnetic field applied perpendicular to the layers and single-ion anisotropy strength (SD) for (a) three layers, (b) four layers, (c) five layers, and (d) six layers. Simulations start in the FM phase at 10 T and the field strength is reduced in equal steps of 0.2 T to −10 T. The solid lines are phase boundaries and metastability limits obtained from the Mills model; the dashed lines are guides to the eye. Collinear phases are labeled as described in the text and noncollinear spin-flop-like phases are labeled as SF. For $N = 6$, panel (d) indicates a metastability limit below which only the M2′ phase is stabilized out of the SF phase.

Much more interesting and complex behavior is obtained for thin films with $N = 6$, where collinear phases appear that have equal uncompensated magnetizations but different symmetries. These phases appear beyond the critical point, as in the $N = 4$ case, which is estimated to be $(SD, \mu_0 H)_\beta =$ (0.084 meV, 3.46 T) from the 6-layer Mills model [35]. Close to the critical point, two different M2 phases appear at positive and negative fields, labeled M2′ and $\overline{\text{M2}''}$ as shown in Fig. 4(d). The mirror symmetric M2′ phase has a single broken AF bond in the center of the stack and is found emerging out of the spin-flop phase (FM → SF → M2′). The mirror symmetry broken $\overline{\text{M2}''}$ has a broken AF bond on the surface and is always stabilized out of the AF state (AF → $\overline{\text{M2}''}$).

The preference for the AF → M2″ transition over the AF → M2′ transition can be understood from metastability arguments related to the barrier height per Mn (E_B) for layer flips that is determined primarily from the uniaxial anisotropy. The AF → M2″ transition requires a coherent spin flip of the surface layer only ($E_B \sim D$), whereas AF → M2′ requires three layer flips ($E_B \sim 3D$). From the FM side, both M2′ and M2″ require two layer flips ($E_B \sim 2D$) and, for this reason, either phase is equally likely to appear above the metastability limit when $D/zJ \gtrsim 0.2$, as indicated by the purple dotted line in Fig. 3(d).

Due to its larger barrier height, M2′ has a lower metastability field to enter the AF phase than M2″ as the field is reduced. To illustrate the metastability limit, Figs. 5(a) and 5(b) show that repeated simulations in which the field is reduced starting from the FM phase will always generate M2′ with $SD = 0.11$ meV, whereas either M2′ or M2″ may appear with $SD = 0.12$ meV. This metastability limit at intermediate D/zJ originates from the intervening spin-flop phase that selectively lowers the barrier to the mirror symmetric M2′ phase when layers 2 and 5 have a large spin-flop angle, as shown in Figs. 5(c)–5(e).

At large D/zJ, metastability issues with the MC simulations reveal that even excited states (such as the M0* state with stacking sequence up-down-up-down-down-up) can be trapped in a local minimum. The occurrence of the M0* phase is dependent on whether the M2′ or M2″ phase appears when lowering the field out of the FM phase. As described above, when the M2″ phase appears, the AF phase is favored since only a spin flip of the surface layer is required. When the M2′ phase appears, transition to the AF phase has a high barrier requiring three layer spin flips. It is therefore more likely for the M2′ phase to transition to the metastable M0* state in which the barrier height is set by a single layer flip. While this large-anisotropy regime is not applicable for $MnBi_2Te_4$,

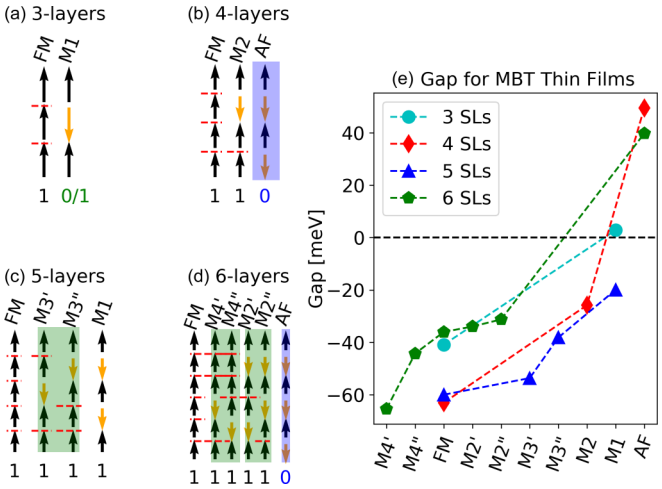

FIG. 4. Possible collinear magnetic ground states for $N = 3$-, 4-, 5-, and 6-layer systems, labeled as either FM, AF, or Mn, where n is the uncompensated net layer magnetization. Red dashed lines indicate broken AF bonds that cost an exchange energy of $3J$ each. Shaded green rectangles enclose degenerate states with the same magnetization but different stacking sequences indicated by the prime symbol. Shaded blue rectangles enclose the states with odd-parity magnetic configuration. The integers below each state denote their Chern numbers calculated from the simplified Dirac-cone model and (e) are the calculated band gaps vs the magnetic stacking sequences of few-layer MBT thin films, here we assigned a negative sign for the phase with nonzero Chern number.

where $D/zJ \approx 0.13$, it may be applicable to $MnBi_4Te_7$ in which nonmagnetic Bi_2Te_3 spacer layers dramatically reduce J.

V. TOPOLOGICAL AND OPTICAL PROPERTIES

A very interesting question is how the stacking sequence of the magnetic layers in MBT thin films and the possible concomitant breaking of symmetries affect observable electronic properties, particularly those related to the topological classification of the electronic structure. To gain insight, we used a simple model of stacked 2D Dirac metals, two for each MBT layer, to calculate the band structure, Chern numbers, and magneto-optical responses of different magnetic states. Previous work [9] has shown that with appropriate coupling between the Dirac metals, models of this type provide a reasonable description of MBT thin films. In this coupled Dirac model, the Hamiltonian is

$$H = \sum_{\mathbf{k}_\perp, ij} [((-)^i \hbar v_D (\hat{z} \times \sigma) \cdot \mathbf{k}_\perp + m_i \sigma_z)\delta_{ij} + \Delta_{ij}(1 - \delta_{ij})] c^\dagger_{\mathbf{k}_\perp i} c_{\mathbf{k}_\perp j}, \quad (2)$$

where the first term is the spin-orbit term while spin labels have been left implicit, Δ_{ij} is the hybridization between the Dirac cones at the surface of septuple layers with i and j the Dirac cone labels, $\hbar$ is the reduced Planck constant, and v_D is the velocity of the Dirac cones. $m_i = \sum_\alpha J_{i\alpha} M_\alpha$ are the mass gaps of individual Dirac cones resulting from exchange interactions with Mn local moments, in which α is a layer label and $M_\alpha = \pm 1$ specifies the direction of the magnetization (up or down) on layer α. The most important hybridization parameters are the hopping within the same septuple layer (Δ_S), hopping across the van der Waals gap between adjacent septuple layers (Δ_D), exchange coupling from Mn moments in the same septuple layer with exchange splitting J_S, and from Mn in the adjacent septuple layer with exchange splitting J_D. In the following, we will retain these four parameters whose values are set to be $\Delta_S = 84$ meV, $\Delta_D = -127$ meV, $J_S = 36$ meV, and $J_D = 29$ meV.

As summarized in Fig. 4, we find that for $N > 3$ all states have unity-magnitude Chern numbers whenever they have uncompensated magnetization, signaling nontrivial topological states. The calculated Chern numbers are listed below each state. The $N = 3$ M1 state is labeled as $0/1$ because it has an extremely small gap and can be on either side of the topological phase transition depending on exchange interaction parameters and on the residual electric field that is likely to be present in any MBT thin films [42]. Odd-layer systems with $N > 3$ are therefore always QAH insulators. The gaps of the various magnetic states we have identified are shown in Fig. 4(e), with a negative sign attached to distinguish cases in which the Chern number is 1 from cases in which the Chern number is 0. The QAH gaps are generally larger for FM magnetic configurations for MBT thin films, except for the M4′ and M4″ states of $N = 6$ films, which have larger gaps than the FM state.

Symmetries play an important role in film electronic properties. We define odd-parity magnetic configurations as ones that have the property that the magnetic moments reverse upon layer reversal. Odd-parity magnetic configurations can be read from the cartoons enclosed with shaded blue rectangles in Fig. 4 and include even N AF configurations. Whenever the magnetic configuration has odd parity, the band Hamiltonian is invariant under the product of time-reversal symmetry $\mathcal{T}$ and inversion symmetry $\mathcal{I}$. (Note that the spin-orbit coupling terms in the coupled Dirac-cone model on the top and bottom surfaces of each septuple layer differ by a sign). For many observables, the consequences of $\mathcal{TI}$ invariance are the same as the consequences separate $\mathcal{T}$ and $\mathcal{I}$ invariance. For example, $\mathcal{TI}$ invariance implies that the Berry curvature $\Omega_n(\mathbf{k}) = -\Omega_n(\mathbf{k}) = 0$. The Berry curvature therefore vanishes identically and a generalized Kramer's theorem implies that all bands are doubly degenerate. It follows that the Chern number vanishes for odd-parity magnetic configurations.

$N = 4$-layer thin films have three possible metamagnetic states (and three time-reversal partners) as shown in Fig. 3(b), i.e., FM, M2′, and AF. $N = 6$-layer thin films host a richer variety of metamagnetic states. We find that all magnetic configurations in $N = 4/6$-layer thin films with a nonzero net spin magnetization (FM, M2′/M2″, or M4′/M4″) have a total Chern number equal to 1 and are therefore QAH insulators. The states cannot be distinguished by performing DC Hall effect measurements. Those properties that are not quantized are distinct for each of these states however. For example, the Berry curvature has a different dependence on momentum in each case, although the total Chern number is always equal to one. As shown in Fig. 6, their optical conductivities differ at finite frequencies. In Figs. 6(a)–6(f) the real and imaginary part of longitudinal optical conductivities $\sigma_{xx}(\omega)$ and transverse optical conductivities $\sigma_{xy}(\omega)$, calculated using

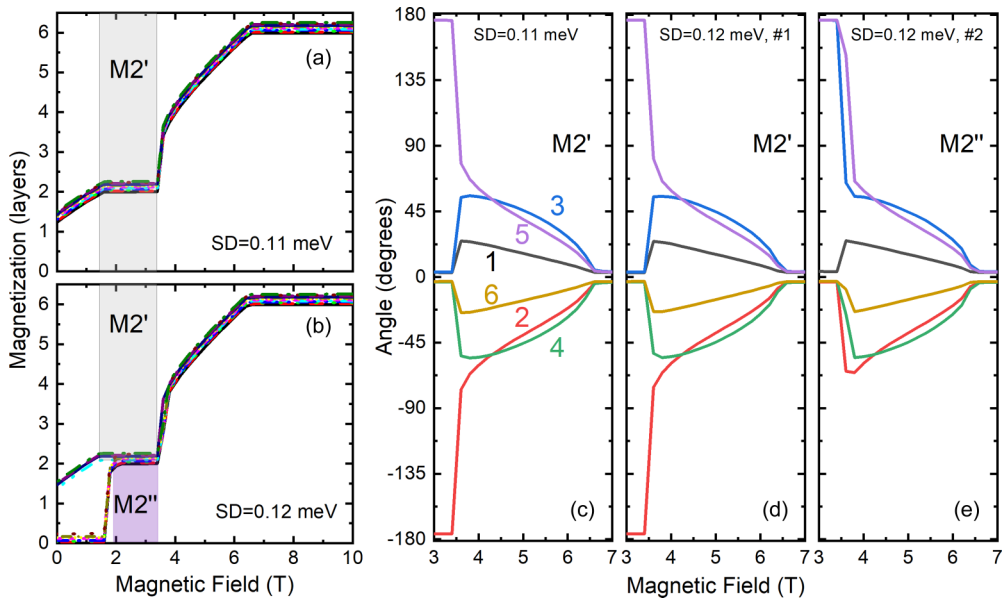

FIG. 5. (a),(b) Twelve MC simulations for $N = 6$ repeated under identical starting conditions near the metastability limit for formation of the M2′ phase. Curves have a slight vertical offset for clarity. (a) For $SD = 0.11$ meV, only the M2′ phase appears. (b) For $SD = 0.12$ meV, either the M2′ or M2″ phase appears. (c)–(e) show the evolution of the magnetization angle for each layer for different simulations. (c) For $SD = 0.11$ meV, which is below the metastability limit, the angle of layers 2 and 5 in the spin-flop phase approaches 90° before flipping into the M2′ phase. For $SD = 0.12$ meV, different simulations (labeled #1 and #2) result in either (d) M2′ with layers 2 and 5 flipping or (e) M2″ with layers 3 and 5 flipping.

the Kubo-Greenwood formula [43,44], are shown. In these plots solid curves represent the real part of the conductivity ($\Re\sigma_{xx/xy}$) while dashed curves represent the corresponding imaginary parts ($\Im\sigma_{xx/xy}$). Each panel represents one metam-

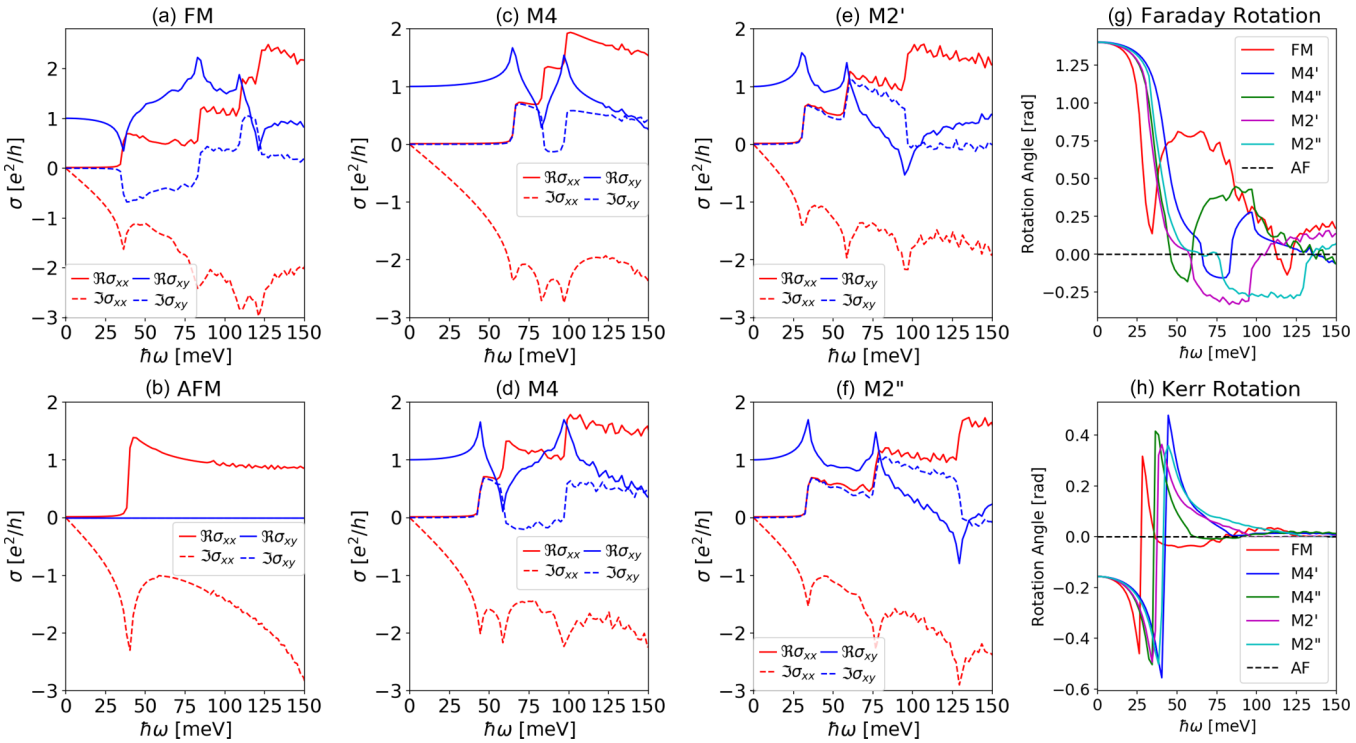

FIG. 6. Nonreciprocal optical response in 6-layer MBT thin films. Panels (a)–(f) show plots of optical longitudinal (σ_{xx}) and Hall (σ_{xy}) conductivities vs optical frequency calculated from the Kubo-Greenwood formula using the simplified Dirac cone electronic structure model. In these plots the solid curves show the real part of a conductivity tensor element while the dashed curves show the imaginary part. In panels (g) and (h), in which the Faraday and Kerr rotation angles in $N = 6$ thin films are plotted vs optical frequency, different colors represent different metamagnetic states.

agnetic state. We show that the external magnetic field drives the 6-layer thin films from their axion insulator states to M2′ or M2″ Chern insulators.

In the DC limit of 6-layer films, Fig. 6 shows that all optical conductivities vanish except for $\Re\sigma_{xy}$ in the case of a QAH insulator. $\Re\sigma_{xx}$ and $\Im\sigma_{xy}$ have peaks when the optical frequencies exceed the two-dimensional band gaps of the thin film. $\Im\sigma_{xx}$ and $\Re\sigma_{xy}$ are, on the other hand, nonzero for frequencies in the thin-film gaps. The frequency dependence of $\Re\sigma_{xy}$ and $\Im\sigma_{xy}$ in the FM states differs from that of other magnetic states in that $\Re\sigma_{xy}$ initially decreases with frequency and $\Im\sigma_{xy}$ is negative below the band gap. This abnormal behavior is caused by the negative Berry curvature around the Γ point in the 2D-band structure.

The optical conductivity tensor components can be converted to frequency-dependent Faraday and Kerr rotation angles commonly measured in experiment. The Faraday and Kerr rotation angles are the relative rotations of left-handed and right-handed circularly polarized light [45] for transmission and reflection, respectively, and these can be connected to the optical conductivity by combining electromagnetic wave boundary conditions and Maxwell equations. The Faraday and Kerr rotation angle vs optical frequency for various metamagnetic states of 6-layer thin film are shown in Figs. 6(g) and 6(h) correspondingly, from which we see that the optical responses of all metamagnetic states with the same Chern number are indistinguishable in the DC limit. As frequency increases, the Faraday and Kerr rotation angles of different metamagnetic states differ substantially. It follows that different metamagnetic states can be distinguished magneto-optically.

VI. DISCUSSION

Generally, $MnBi_2Te_4$ (MBT) thin films with uncompensated magnetic layers are topologically nontrivial. For N odd and larger than 3, all collinear MBT thin film states are QAH insulators. For even N, the ground states are axion insulators in the absence of an external magnetic field. In our studies, we have identified the metamagnetic states that can be induced in MBT thin films with up to $N = 6$ septuple layers by applying external magnetic fields. Collinear metamagnetic states that are Chern insulators can be induced by applying external magnetic field provided that the single-ion magnetic anisotropy is large enough compared with the interlayer exchange interactions. Both M2 and M4 states are Chern insulators with QAH gaps comparable to those of the FM state for 4-layer and 6-layer thin films, and they appear at much smaller magnetic fields. These metamagnetic states are not distinguished in transport experiments since they all have the same Chern number as the FM state. However, they may be distinguished by their magneto-optical Kerr and Faraday rotation angles.

Thicker films, especially for even-layer systems and for the thin films with high Chern number FM states (that is $N = 9$ layers thick or thicker), await further exploration. Interesting questions arise when the thickness increases: Is it possible, for example, to have a high-Chern-number state at a weaker magnetic field? For MBT thin films the magnetic anisotropy seems to be comparable with the interlayer exchange interaction; it may therefore be interesting to explore other intrinsic magnetic topological insulators, such as $MnBi_4Te_7$ that have relatively larger magnetic anisotropy to induce more metamagnetic states, or to find tools, such as electric field, that may increase the magnetic anisotropy.

ACKNOWLEDGMENTS

R.J.M. and O.H. were supported by the Center for the Advancement of Topological Semimetals, an Energy Frontier Research Center funded by the US Department of Energy Office of Science, Office of Basic Energy Sciences, through the Ames Laboratory under Contract No. DE-AC02-07CH11358. C.L. and A.H.M. were supported by the Army Research Office under Grant No. W911NF-16-1-0472. O.H. gratefully acknowledges the computing resources provided on Bebop and Blues, high-performance computing clusters operated by the Laboratory Computing Resource Center at Argonne National Laboratory.

[1] S. V. Eremeev, M. M. Otrokov, and E. V. Chulkov, Competing rhombohedral and monoclinic crystal structures in $MnPn_2Ch_4$ compounds: An *ab-initio* study, J. Alloys Compd. **709**, 172 (2017).

[2] M. M. Otrokov, T. V. Menshchikova, M. G Vergniory, I. P. Rusinov, A. Yu Vyazovskaya, Yu. M. Koroteev, G. Bihlmayer, A. Ernst, P. M. Echenique, A. Arnau *et al.*, Highly-ordered wide bandgap materials for quantized anomalous Hall and magnetoelectric effects, 2D Materials **4**, 025082 (2017).

[3] M. M. Otrokov, I. I. Klimovskikh, H. Bentmann, D. Estyunin, A. Zeugner, Z. S. Aliev, S. Gaß, A. U. B. Wolter, A. V. Koroleva, A. M. Shikin *et al.*, Prediction and observation of an antiferromagnetic topological insulator, Nature (London) **576**, 416 (2019).

[4] E. D. L. Rienks, S. Wimmer, J. Sánchez-Barriga, O. Caha, P. S. Mandal, J. Røužička, A. Ney, H. Steiner, V. V. Volobuev, H. Groiss *et al.*, Large magnetic gap at the dirac point in $Bi_2Te_3/MnBi_2Te_4$ heterostructures, Nature (London) **576**, 423 (2019).

[5] Y. J. Chen, L. X. Xu, J. H. Li, Y. W. Li, H. Y. Wang, C. F. Zhang, H. Li, Y. Wu, A. J. Liang, C. Chen, S. W. Jung, C. Cacho, Y. H. Mao, S. Liu, M. X. Wang, Y. F. Guo, Y. Xu, Z. K. Liu, L. X. Yang, and Y. L. Chen, Topological Electronic Structure and Its Temperature Evolution in Antiferromagnetic Topological Insulator $MnBi_2Te_4$, Phys. Rev. X **9**, 041040 (2019).

[6] Y.-J. Hao, P. Liu, Y. Feng, X.-M. Ma, E. F. Schwier, M. Arita, S. Kumar, C. Hu, R. Lu, M. Zeng, Y. Wang, Z. Hao, H.-Y. Sun, K. Zhang, J. Mei, N. Ni, L. Wu, K. Shimada, C. Chen, Q. Liu, and C. Liu, Gapless Surface Dirac Cone in Antiferromagnetic Topological Insulator Bi_2Te_4, Phys. Rev. X **9**, 041038 (2019).

[7] H. Li, S.-Y. Gao, S.-F. Duan, Y.-F. Xu, K.-J. Zhu, S.-J. Tian, J.-C. Gao, W.-H. Fan, Z.-C. Rao, J.-R. Huang, J.-J. Li, D.-Y. Yan, Z.-T. Liu, W.-L. Liu, Y.-B. Huang, Y.-L. Li, Y. Liu, G.-B. Zhang, P. Zhang, T. Kondo, S. Shin, H.-C. Lei, Y.-G. Shi,

W.-T. Zhang, H.-M. Weng, T. Qian, H. Ding *et al.*, Dirac Surface States in Intrinsic Magnetic Topological Insulators $EuSn_2As_2$ and $MnBi_{2n}Te_{3n+1}$, Phys. Rev. X **9**, 041039 (2019).

[8] P. Swatek, Y. Wu, L.-L. Wang, K. Lee, B. Schrunk, J. Yan, and A. Kaminski, Gapless Dirac surface states in the antiferromagnetic topological insulator $MnBi_2Te_4$, Phys. Rev. B **101**, 161109(R) (2020).

[9] C. Lei, S. Chen, and A. H. MacDonald, Magnetized topological insulator multilayers, Proc. Natl. Acad. Sci. **117**, 27224 (2020).

[10] S. H. Lee, Y. Zhu, Y. Wang, L. Miao, T. Pillsbury, H. Yi, S. Kempinger, J. Hu, C. A. Heikes, P. Quarterman, W. Ratcliff, J. A. Borchers, H. Zhang, X. Ke, D. Graf, N. Alem, C.-Z. Chang, N. Samarth, and Z. Mao, Spin scattering and noncollinear spin structure-induced intrinsic anomalous Hall effect in antiferromagnetic topological insulator $MnBi_2Te_4$, Phys. Rev. Research **1**, 012011(R) (2019).

[11] Y. Deng, Y. Yu, M. Z. Shi, Z. Guo, Z. Xu, J. Wang, X. H. Chen, and Y. Zhang, Quantum anomalous Hall effect in intrinsic magnetic topological insulator $MnBi_2Te_4$, Science **367**, 895 (2020).

[12] Y. Gong, J. Guo, J. Li, K. Zhu, M. Liao, X. Liu, Q. Zhang, L. Gu, L. Tang, X. Feng *et al.*, Experimental realization of an intrinsic magnetic topological insulator, Chin. Phys. Lett. **36**, 076801(R) (2019).

[13] D. Zhang, M. Shi, T. Zhu, D. Xing, H. Zhang, and J. Wang, Topological Axion States in the Magnetic Insulator $MnBi_2Te_4$ with the Quantized Magnetoelectric Effect, Phys. Rev. Lett. **122**, 206401 (2019).

[14] I. I. Klimovskikh, M. M. Otrokov, D. Estyunin, S. V. Eremeev, S. O. Filnov, A. Koroleva, E. Shevchenko, V. Voroshnin, A. G. Rybkin, I. P. Rusinov *et al.*, Tunable 3D/2D Magnetism in the $(MnBi_2Te_4)(Bi_2Te_3)_m$ Topological Insulators Family, npj Quantum Mater. **5**, 54 (2020).

[15] J. Li, Y. Li, S. Du, Z. Wang, B.-L. Gu, S.-C. Zhang, K. He, W. Duan, and Y. Xu, Intrinsic magnetic topological insulators in van der Waals layered $MnBi_2Te_4$-family materials, Sci. Adv. **5**, eaaw5685 (2019).

[16] S. Chowdhury, K. F. Garrity, and F. Tavazza, Prediction of Weyl semimetal and antiferromagnetic topological insulator phases in Bi_2MnSe_4, npj Comput. Mater. **5**, 33 (2019).

[17] B. Li, J.-Q. Yan, D. M. Pajerowski, E. Gordon, A.-M. Nedić, Y. Sizyuk, L. Ke, P. P. Orth, D. Vaknin, and R. J. McQueeney, Competing Magnetic Interactions in the Antiferromagnetic Topological nsulator $MnBi_2Te_4$, Phys. Rev. Lett. **124**, 167204 (2020).

[18] J.-Q. Yan, Q. Zhang, T. Heitmann, Z. Huang, K. Y. Chen, J.-G. Cheng, W. Wu, D. Vaknin, B. C. Sales, and R. J. McQueeney, Crystal Growth and Magnetic Structure of $MnBi_2Te_4$, Phys. Rev. Mater. **3**, 064202 (2019).

[19] A. Zeugner, F. Nietschke, A. U. B. Wolter, S. Gaß, R. C. Vidal, T. R. F. Peixoto, D. Pohl, C. Damm, A. Lubk, R. Hentrich *et al.*, Chemical aspects of the candidate antiferromagnetic topological insulator $MnBi_2Te_4$, Chem. Mater. **31**, 2795 (2019).

[20] J. Wu, F. Liu, M. Sasase, K. Ienaga, Y. Obata, R. Yukawa, K. Horiba, H. Kumigashira, S. Okuma, T. Inoshita *et al.*, Natural van der waals heterostructural single crystals with both magnetic and topological properties, Sci. Adv. **5**, eaax9989 (2019).

[21] S. Zhang, R. Wang, X. Wang, B. Wei, B. Chen, H. Wang, G. Shi, F. Wang, B. Jia, Y. Ouyang *et al.*, Experimental observation of the gate-controlled reversal of the anomalous Hall effect in the intrinsic magnetic topological insulator $MnBi_2Te_4$ device, Nano Lett. **20**, 709 (2019).

[22] M. M. Otrokov, I. P. Rusinov, M. Blanco-Rey, M. Hoffmann, A. Yu. Vyazovskaya, S. V. Eremeev, A. Ernst, P. M. Echenique, A. Arnau, and E. V. Chulkov, Unique Thickness-Dependent Properties of the van der Waals Interlayer Antiferromagnet $MnBi_2Te_4$ Films, Phys. Rev. Lett. **122**, 107202 (2019).

[23] C. Liu, Y. Wang, H. Li, Y. Wu, Y. Li, J. Li, K. He, Y. Xu, J. Zhang, and Y. Wang, Robust axion insulator and chern insulator phases in a two-dimensional antiferromagnetic topological insulator, Nat. Mater. **19**, 522 (2020).

[24] K. Y. Chen, B. S. Wang, J.-Q. Yan, D. S. Parker, J.-S. Zhou, Y. Uwatoko, and J.-G. Cheng, Suppression of the antiferromagnetic metallic state in the pressurized $MnBi_2Te_4$ single crystal, Phys. Rev. Mater. **3**, 094201 (2019).

[25] L. Ding, C. Hu, F. Ye, E. Feng, N. Ni, and H. Cao, Crystal and magnetic structures of magnetic topological insulators $MnBi_2Te_4$ and $MnBi_4Te_7$, Phys. Rev. B **101**, 020412(R) (2020).

[26] R. C. Vidal, A. Zeugner, J. I. Facio, R. Ray, M. H. Haghighi, A. U. B. Wolter, L. T. CorredorBohorquez, F. Caglieris, S. Moser, T. Figgemeier, T. R. F. Peixoto, H. B. Vasili, M. Valvidares, S. Jung, C. Cacho, A. Alfonsov, K. Mehlawat, V. Kataev, C. Hess, M. Richter, B. Buchner, J. van den Brink, M. Ruck, F. Reinert, H. Bentmann, and A. Isaeva, Topological Electronic Structure and Intrinsic Magnetization in $MnBi_4Te_7$: A Bi_2Te_3 Derivative with a Periodic Mn Sublattice, Phys. Rev. X **9**, 041065 (2019).

[27] R. C. Vidal, H. Bentmann, T. R. F. Peixoto, A. Zeugner, S. Moser, C.-H. Min, S. Schatz, K. Kißner, M. Ünzelmann, C. I. Fornari, H. B. Vasili, M. Valvidares, K. Sakamoto, D. Mondal, J. Fujii, I. Vobornik, S. Jung, C. Cacho, T. K. Kim, R. J. Koch, C. Jozwiak, A. Bostwick, J. D. Denlinger, E. Rotenberg, J. Buck, M. Hoesch, F. Diekmann, S. Rohlf, M. Kalläne, K. Rossnagel, M. M. Otrokov, E. V. Chulkov, M. Ruck, A. Isaeva, and F. Reinert, Surface states and Rashba-type spin polarization in antiferromagnetic $MnBi_2Te_4$(0001), Phys. Rev. B **100**, 121104(R) (2019).

[28] J. Ge, Y. Liu, J. Li, H. Li, T. Luo, Y. Wu, Y. Xu, and J. Wang, High-chern-number and high-temperature quantum Hall effect without landau levels, Natl. Sci. Rev. **7**, 1280 (2020).

[29] A. M. Essin, J. E. Moore, and D. Vanderbilt, Magnetoelectric Polarizability and Axion Electrodynamics in Crystalline Insulators, Phys. Rev. Lett. **102**, 146805 (2009).

[30] R. S. K. Mong, A. M. Essin, and J. E. Moore, Antiferromagnetic topological insulators, Phys. Rev. B **81**, 245209 (2010).

[31] H. Deng, Z. Chen, A. Wołoś, M. Konczykowski, K. Sobczak, J. Sitnicka, I. V. Fedorchenko, J. Borysiuk, T. Heider, Ł. Pluciński *et al.*, High-temperature quantum anomalous Hall regime in a $MnBi_2Te_4/Bi_2Te_3$ superlattice, Nat. Phys. **17**, 36 (2020).

[32] D. Ovchinnikov, X. Huang, Z. Lin, Z. Fei, J. Cai, T. Song, M. He, Q. Jiang, C. Wang, H. Li *et al.*, Intertwined topological and magnetic orders in atomically thin chern insulator $MnBi_2Te_4$, Nano Lett. **21**, 2544 (2021).

[33] S. Yang, X. Xu, Y. Zhu, R. Niu, C. Xu, Y. Peng, X. Cheng, X. Jia, Y. Huang, X. Xu, J. Lu, Y. Ye, Odd-Even Layer-Number Effect and Layer-Dependent Magnetic Phase Diagrams in $MnBi_2Te_4$, Phys. Rev. X **11**, 011003 (2020).

[34] O. Hellwig, T. L. Kirk, J. B. Kortright, A. Berger, and E. E. Fullerton, A new phase diagram for layered antiferromagnetic films, Nat. Mater. **2**, 112 (2003).

[35] U. K. Rößler and A. N. Bogdanov, Reorientation in antiferromagnetic multilayers: Spin-flop transition and surface effects, Physica Status Solidi A **1**, 3297 (2004).

[36] B. Skubic, J. Hellsvik, L. Nordström, and O. Eriksson, A method for atomistic spin dynamics simulations: Implementation and examples, J. Phys.: Condens. Matter **20**, 315203 (2008).

[37] R. F. L. Evans, W. J. Fan, P. Chureemart, T. A. Ostler, M. O. A. Ellis, and R. W. Chantrell, Atomistic spin model simulations of magnetic nanomaterials, J. Phys.: Condens. Matter **26**, 103202 (2014).

[38] P. M. Sass, J. Kim, D. Vanderbilt, J. Yan, and W. Wu, Robust A-Type Order and Spin-Flop Transition on the Surface of the Antiferromagnetic Topological Insulator $MnBi_2Te_4$, Phys. Rev. Lett. **125**, 037201 (2020).

[39] A. Tan, V. Labracherie, N. Kunchur, A. U. B. Wolter, J. Cornejo, J. Dufouleur, B. Büchner, A. Isaeva, and R. Giraud, Metamagnetism of Weakly Coupled Antiferromagnetic Topological Insulators, Phys. Rev. Lett. **124**, 197201 (2020).

[40] J. Wu, F. Liu, C. Liu, Y. Wang, C. Li, Y. Lu, S. Matsuishi, and H. Hosono, Toward 2D magnets in the $(MnBi_2Te_4)(Bi_2Te_3)_n$ bulk crystal, Adv. Mater. **32**, 2001815 (2020).

[41] D. L. Mills, Surface Spin-Flop State in a Simple Antiferromagnet, Phys. Rev. Lett. **20**, 18 (1968).

[42] C. Lei and A. H. MacDonald, Gate-tunable quantum anomalous hall effects in $MnBi_2Te_4$ thin films, Phys. Rev. Materials **5**, L051201 (2021).

[43] R. Kubo, Statistical-mechanical theory of irreversible processes. I. general theory and simple applications to magnetic and conduction problems, J. Phys. Soc. Jpn. **12**, 570 (1957).

[44] D. A. Greenwood, The Boltzmann equation in the theory of electrical conduction in metals, Proc. Phys. Soc. (1958-1967) **71**, 585 (1958).

[45] W.-K. Tse and A. H. MacDonald, Magneto-optical faraday and Kerr effects in topological insulator films and in other layered quantized Hall systems, Phys. Rev. B **84**, 205327 (2011).